energies

MDPI

Article

Assessment of Offshore Wind Characteristics and Wind Energy Potential in Bohai Bay, China

Jianxing Yu [1,2], Yiqin Fu [1,2,*], Yang Yu [1,2], Shibo Wu [1,2], Yuanda Wu [1,2], Minjie You [1,2], Shuai Guo [1,2] and Mu Li [3]

[1] State Key Laboratory of Hydraulic Engineering Simulation and Safety, Tianjin University, Tianjin 300072, China
[2] Collaborative Innovation Center for Advanced Ship and Deep-Sea Exploration, Shanghai 200240, China
[3] CNOOC Energy Technology & Services-Oil Production Services, Bohai Oil Road No. 688, Tanggu, Tianjin 300451, China
* Correspondence: fuyiqin@tju.edu.cn

Received: 8 July 2019; Accepted: 23 July 2019; Published: 26 July 2019

Abstract: Wind energy, one of the most sustainable renewable energy sources, has been extensively developed worldwide. However, owing to the strong regional and seasonal differences, it is necessary to first evaluate wind energy resources in detail. In this study, the offshore wind characteristics and wind energy potential of Bohai Bay (38.7° N, 118.7° E), China, were statistically analyzed using two-year offshore wind data with a time interval of one second. Furthermore, Nakagami and Rician distributions were used for wind energy resource assessment. The results show that the main wind direction in Bohai Bay is from the east (−15°–45°), with a speed below 12 m/s, mainly ranging from 4 to 8 m/s. The main wind speed ranges in April and October are higher than those in August and December. The night wind speed is generally higher than that in the daytime. The Nakagami and Rician distributions performed reasonably in calculating the wind speed distributions and potential assessments. However, Nakagami distribution provided better wind resource assessment in this region. The wind potential assessment results suggest that Bohai Bay could be considered as a wind class I region, with east as the dominant wind direction.

Keywords: statistical analysis; wind energy; Nakagami distribution; Rician distribution; Bohai Bay

1. Introduction

Wind energy is currently the most competitively priced technology in many markets, and China leads the wind power market. Over 52 GW of clean, emissions-free wind power was installed in 2017, bringing the total global installation to 539 GW [1]. However, unlike its onshore wind counterparts in Gansu, Xinjiang Jilin, and Inner Mongolia, the first 1000 MW/year of offshore wind in China was installed only in 2017 owing to the great cost of constructing, maintaining, and repairing offshore wind turbines [1]. Zhao [2] claimed that the "golden period" of offshore wind power will arrive in 2020, based on their analysis of Chinese policies, markets, technology, and development plans. The Chinese government is expected to substantially expand the offshore wind market over the next few years [1].

Although wind power, as one of the most sustainable renewable energies, is abundant, it requires the in-depth analysis of wind characteristics and potential in order to determine the feasibility of installing offshore wind turbines [3,4].

As the demand for renewable energy is rapidly increasing, the Chinese government has focused on the potential for offshore wind power in Bohai Bay, and it is imperative to understand the wind characteristics and potential in advance. Wind characteristics include its speed and direction. Many studies have described these characteristics using an adequate statistical model, and the probability

density functions (PDFs) are among the most suitable models for estimating wind power density [5–9]. Recently, an increasing number of researchers have attempted to assess the feasibility of installing offshore wind power farms in different parts of China [10], such as the waters around Hong Kong [11,12], the Bohai Rim Economic circle [13], the East China Sea [14], and the South China Sea [15,16].

This study aimed to assess wind characteristics using the wind data measured in Bohai Bay (38.7° N, 118.7° E) by Weibull, Nakagami, Rician, and Rayleigh distributions. Nakagami and Rician distributions were first used to analyze the wind characteristics, and they exhibited a reasonable performance in forecasting wind speed distributions and conducting wind potential assessments. This aids in the production of an efficient plan for installing offshore wind power farms in Bohai Bay.

2. Wind Data Analysis Methods

Many two-parameter PDFs have been employed to evaluate the potential of wind energy resources, such as the Weibull, lognormal, gamma, and Gumbel PDFs [17]. However, the Weibull and Raleigh distributions are two of the most suitable and widely used tools for assessing wind potential [18,19]. Hennessey [20], Deaves and Lines [21], and Kumar [22] improved the Weibull PDF to accurately represent wind speed and estimate wind potential. Carta et al. [23] compared the Weibull PDF to 12 other probability density models and found that Weibull PDF has several advantages in terms of its flexibility and accuracy. Wais [8] developed the Weibull PDF to allow it to be used for null wind, while Ali et al. [4] used the two-parameter Weibull and Rayleigh PDFs to estimate the wind energy potential in South Korea. Chang et al. [24] and Jiang et al. [25] employed different PDFs, including the Weibull PDF, to estimate the wind energy potential in Taiwan and the Yangtze River Delta City Group in China, respectively.

Nakagami (Nakagami-m) distribution was first proposed in 1960 for studying signal wave propagation. It was then gradually applied for different functions [26], such as signal-to-noise ratio estimation [27], fading channel [28], quantitative ultrasound imaging [29], and so on. Rician (Nakagami-n) distribution was first proposed in 1945 in the fields of information theory, communication theory, and telecommunication, which are the same application fields as those for Nakagami distribution [30,31]. To date, there has been no relevant research regarding Nakagami (Rician) distribution in the field of wind energy resource assessment.

According to previous studies, there are mathematical approaches to estimate the distribution parameters, such as the least-squares, maximum likelihood, moment, and empirical methods [6,25]. The distribution parameters should be determined as accurately as possible to indicate the abscissa and ordinate ranges of wind speed data [4]. Parameter estimation is not the focus of this study and will be discussed in further research. In this study, the parameters were calculated by nonlinear least-squares methods using MATLAB software. In this section, the Nakagami and Rician distributions are first examined for assessing wind energy resources. In Section 4, these two functions are reviewed and compared to the conventional Weibull and Rayleigh functions for fitting wind speed distributions and assessing wind energy potential.

2.1. Weibull Distribution

The general form of the two-parameter Weibull PDF is written as follows [4]:

$$f_{Wei}(k,c,v) = \left(\frac{k}{c}\right)\left(\frac{v}{c}\right)^{k-1} e^{-\left(\frac{v}{c}\right)^k} (v > 0,\ c > 0) \quad (1)$$

where $f(v)$ is the probability of the observed wind speed v (m/s), k is the shape parameter (dimensionless), and c is the scale parameter (m/s). The corresponding cumulative distribution function (CDF) is as follows:

$$F_{Wei}(k,c,v) = 1 - e^{-\left(\frac{v}{c}\right)^k} \quad (2)$$

where $F(v)$ represents the probability of all wind speeds less than v.

2.2. Nakagami Distribution

The Nakagami distribution (or Nakagami-m distribution) is a probability distribution related to the gamma distribution, which has two parameters, i.e., a shape parameter $\mu \geq 1/2$ and a scale parameter $\omega > 0$ controlling spread. Its PDF and CDF are as follows:

$$f_{Nak}(\mu, \omega, v) = 2(\frac{\mu}{\omega})^{\mu} \frac{1}{\Gamma(\mu)} v^{(2\mu-1)} e^{-\frac{\mu v^2}{\omega}} \tag{3}$$

$$F_{Nak}(\mu, \omega, v) = \frac{\gamma\left(\mu, \frac{\mu}{\omega} v^2\right)}{\Gamma(\mu)} \tag{4}$$

where $f_{Nkg}(v)$ and $F_{Nkg}(v)$ are the PDF and the CDF of observed wind speed v, respectively, and $\Gamma(x)$ is the gamma function:

$$\Gamma(x) = \int_0^{\infty} t^{x-1} e^{-t} dt \tag{5}$$

$\gamma(\mu, \frac{\mu}{\omega} v^2)$ is the upper incomplete gamma function:

$$\gamma(\mu, \frac{\mu}{\omega} v^2) = \int_{\frac{\mu}{\omega} v^2}^{\infty} t^{\mu-1} e^{-t} dt \tag{6}$$

2.3. Rician Distribution

Rician distribution (or the Nakagami-n distribution) is the probability distribution of the magnitude of a circular bivariate normal random variable with potential nonzero mean [30]. Its PDF is as follows:

$$f_{Ric}(a, b, v) = \frac{v}{a^2} e^{\frac{-(v^2+b^2)}{2a^2}} I_0(\frac{bv}{a^2}) \ (a \geq 0, \ b \geq 0) \tag{7}$$

where a and b are the scale and location parameters of Rician distribution, respectively. b is the distance between the reference point and centre of the bivariate distribution, and $I_0(z)$ is the modified Bessel function of the first-kind $I_\alpha(z)$ with an order of zero, where

$$I_\alpha(z) = \sum_{k=0}^{\infty} \frac{\left(\frac{z}{2}\right)^{2k+\alpha}}{k!\Gamma(k+\alpha+1)} \tag{8}$$

Its CDF is as follows:

$$F_{Ric}(a, b, v) = 1 - Q_1\left(\frac{b}{a}, \frac{v}{a}\right) \tag{9}$$

where $Q_1\left(\frac{b}{a}, \frac{v}{a}\right)$ is the Marcum Q-function:

$$Q_1(\frac{b}{a}, \frac{v}{a}) = \int_{v/a}^{\infty} x e^{-\frac{x^2+b^2/a^2}{2}} I_0(\frac{bx}{a}) dx \tag{10}$$

2.4. Rayleigh Distribution

The Rayleigh distribution, a one-parameter continuous probability distribution, is a special form of Weibull distribution with a shape parameter k of 2. Its PDF and CDF are as follows [4]:

$$f_{ray}(v; \sigma) = \frac{x}{\sigma^2} e^{-\frac{v^2}{2\sigma^2}} \tag{11}$$

$$F_{ray}(v;\sigma) = 1 - e^{-\frac{v^2}{2\sigma^2}} \tag{12}$$

where σ is the scale parameter, and v is the observed speed.

2.5. Coefficient of Determination

The correlation coefficient (R^2) and root mean square error (RMSE) were used to determine the performance of different distributions. R^2 is the statistical relationship between two variables, which is expressed by the proportion of variance in the dependent variable that is predictable from the independent variables, while RMSE is a frequently used measure of the differences between the values predicted by a model and the observed values. These can be calculated as follows [6]:

$$\text{RMSE} = \sqrt{\frac{1}{m}\sum_{i=1}^{m}(y_i - \hat{y}_i)^2} \tag{13}$$

$$R = \sqrt{1 - \frac{\sum_{i=1}^{m}(y_i - \hat{y}_i)^2}{\sum_{i=1}^{m}(y_i - \overline{y})^2}} \tag{14}$$

where y_i is the observed data in the ith bin, $\hat{y}_i$ is the corresponding predicted value, $\overline{y}$ is the mean of the total observed data, and m is the number of bins. More accurate predicted models have higher correlation coefficient R values and lower RMSE values.

3. Wind Data

Although it is easier to install wind energy generators onshore, offshore wind energy is more attractive as it is more reliable and consistent [32]. As wind is highly temporally variable, detailed analysis of wind characteristics should be conducted at different timescales, such as seasons, months, and hours.

Figure 1 shows the wind data collected from the wind anemoscope installed on the top of 'HYSY112' floating production storage and offloading (FPSO) unit, which remained at the same location around the single point mooring system in the western part of Bohai Bay (38.7° N, 118.7° E), China, approximately 90 km west of Tianjin Xingang Port at a depth of 20 m (as shown in Figure 2). The wind data used in this study were supported by the China National Offshore Oil Corporation (CNOOC) Energy Technology & Services Limited. The height of the anemometer was approximately 60 m above sea level, which is similar to the height of offshore wind turbines. The wind data, including the wind speed and direction, were recorded from March 2015 to March 2017 with an interval of one second. Wind data should be measured for at least one year to increase the reliability of the results, which is also the baseline for wind power projects [33]. Table 1 provides in brief the parameters of the measuring apparatus. As the measuring region is far away from the public, noise was not considered.

Figure 1. Measuring apparatus and its surrounding environment.

Figure 2. Bohai Bay and the location of the floating production storage and offloading (FPSO) unit (from Google Earth).

Table 1. Wind data collected by the measurement sensors.

Location	Latitude	Longitude	Begin	End	Height (m)	Interval	Recovery Rate
Bohai Bay	38.7° N	118.7° E	2015.03	2017.05	60	1 s	96%

The Bohai Bay region experiences a temperate monsoon climate with clear seasonal variations. The summer is very hot and humid, while the winter is extremely cold and dry. In this study, the wind data have been divided into three groups according to the season (four seasons), month (12 months), and hour (24 h) the data were collected in to better understand the wind behavior. The seasons are defined as follows:

(1) Spring: March–May;
(2) Summer: June–August;
(3) Autumn: September–November;
(4) Winter: December–February.

4. Results and Discussion

The detailed statistical analyses of the wind data collected during different time periods are presented in Section 4.1. The wind rose diagram can be used to understand both the wind speed and direction. Turbulence intensity (TI) at each wind speed range and different periods can help us classify wind turbines. The prevailing wind direction in Bohai Bay can be determined easily, so the optimal position of wind turbine projects can be determined in the future. PDFs are introduced to fit the wind speed distribution and conduct the wind energy potential analysis in Sections 4.2 and 4.3.

4.1. Statistical Analysis of Wind Data

Figure 3 shows the main wind direction and wind speed magnitudes, along with the seasonal variations. Tables 2 and 3 show the total observed annual, seasonal, and monthly wind speed ranges (WSRs).

The main wind speed ranges exhibit two wave motion patterns throughout the year. The main wind speed ranges are 2–5 m/s in December and August and 4–9 m/s in April and October. Almost 98% of the winds are below 12 m/s, 70% of which are within in the range of 2–8 m/s; separated by season, this percentage is 72.83% in spring, 82.29% in summer, 73.88% in autumn, and 73.98% in winter.

The percentages of gales (wind speed >12 m/s) in autumn and winter are higher than those in spring and summer.

The main wind direction is from the (E −15°–45°), followed by the southeast (SE −55°–−45°) and northeast (NE 55°–75°). The wind directions in spring, autumn, and winter are very similar, while the probability of the easterly winds in summer is lower than that in the other seasons. The prevailing wind direction is from the Pacific Ocean to the land, which may be due to the temperate monsoon climate of Bohai Bay [4].

Tables 4 and 5 show that the mean wind speed (MWS) in summer is relatively lower than that during the other seasons, but the corresponding extreme wind speed (EWS) is higher than that during the other seasons due to the typhoons and seasonal monsoons that occur in the summer. The EWS events could be negligible for wind resource assessment because the EWS events (>24.7 m/s) lasted less than 19 min in two years. In spring, the MWS is relatively higher, and the standard deviation (SD) is lower than that during the other seasons. Therefore, during spring, wind energy could be used more effectively. The monthly MWS exhibits the same tendency as the main wind speed ranges. The minimum and maximum MWS values occur in August and April, respectively. The monthly SDs are stable at approximately 2.3 from February to September and then exceed 3.1 from October to January. This may be due to the winter monsoon originating in Mongolia and Siberia, which has a higher pressure than the summer monsoon originating in the Pacific Ocean due to the differences between the thermal properties of the land and sea.

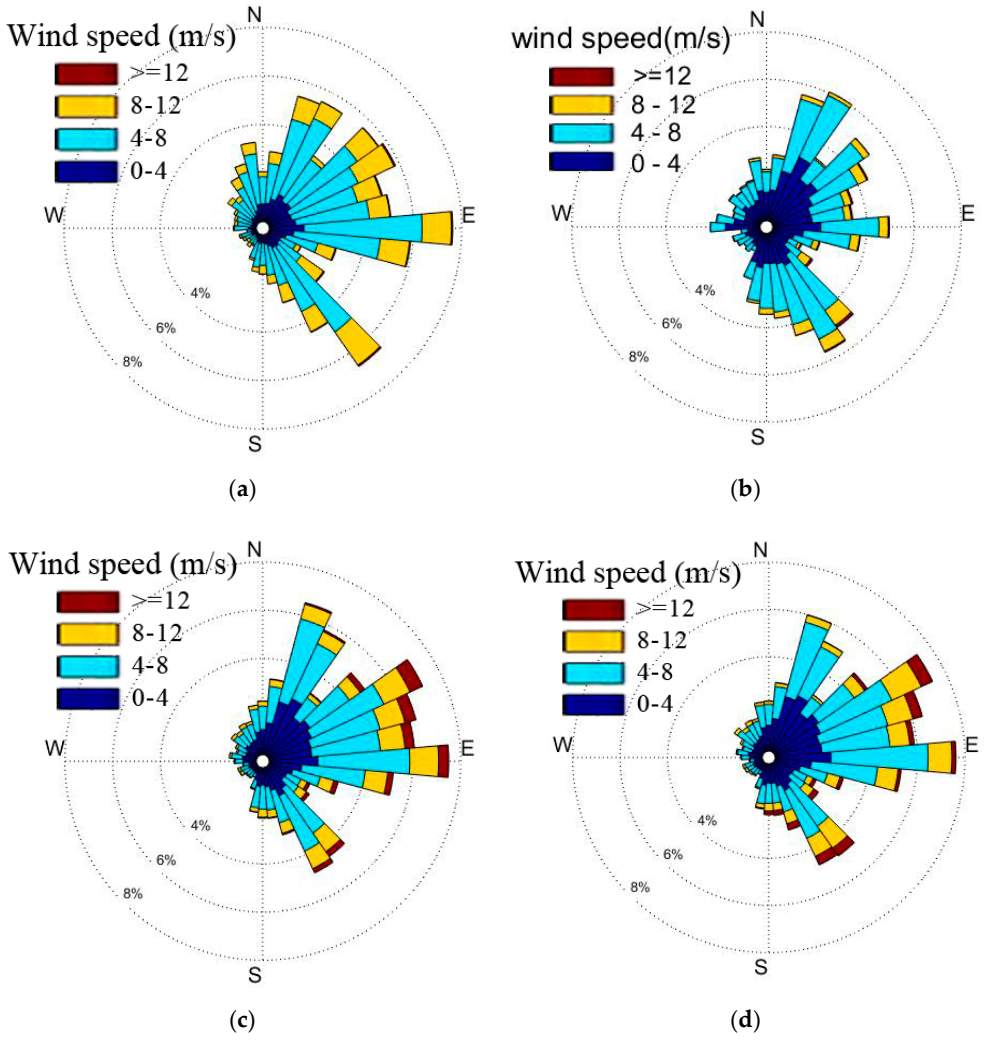

Figure 3. Wind roses: (**a**) spring; (**b**) summer; (**c**) autumn; (**d**) winter.

Table 2. Percentages of the annual and seasonal wind speed ranges (WSRs).

WSR (m/s)	Percentage of Total Wind Occurrence (%)					
	Spring	**Summer**	**Autumn**	**Winter**	**Annual**	**Sum**
[0,1)	0.81	3.43	1.48	1.53	1.82	1.82
[1,2)	2.30	5.10	4.59	5.43	4.38	6.20
[2,3)	5.46	12.65	11.23	11.99	10.39	16.59
[3,4)	7.95	16.66	13.77	14.14	13.19	29.78
[4,5)	11.77	17.92	14.15	14.73	14.27	44.45
[5,6)	15.15	15.20	13.62	13.15	12.54	58.72
[6,7)	16.29	11.60	11.46	10.99	10.71	71.26
[7,8)	16.21	8.26	9.65	8.98	6.64	81.97
[8,9)	10.63	4.03	6.19	5.89	4.38	88.61
[9,10)	7.09	2.15	4.37	4.03	2.70	92.99
[10,11)	3.72	1.25	3.06	2.80	1.59	95.69
[11,12)	1.59	0.78	2.05	1.95	1.04	97.28
[12,13)	0.67	0.45	1.50	1.51	0.57	98.32
[13,14)	0.19	0.20	0.90	0.97	0.38	98.89
[14,15)	0.09	0.12	0.62	0.69	0.27	99.27
[15,16)	0.04	0.08	0.44	0.50	0.18	99.54
[16,17)	0.02	0.06	0.32	0.33	0.13	99.72
[17, ∞)	0.01	0.09	0.62	0.40	0.15	100

Table 3. Percentages of the monthly WSRs.

WRS (m/s)	Percentage of Total Wind Occurrence											
	Jan	**Feb**	**Mar**	**Apr**	**May**	**Jun**	**Jul**	**Aug**	**Sep**	**Oct**	**Nov**	**Dec**
[0,1)	1.53	1.32	0.76	1.00	0.68	1.74	3.02	5.62	2.77	0.74	0.80	1.71
[1,2)	5.59	4.14	2.31	2.30	2.29	3.25	4.86	7.23	6.93	3.11	3.55	6.41
[2,3)	12.55	9.59	6.44	4.97	5.09	6.88	12.23	18.94	15.53	8.05	9.87	13.55
[3,4)	14.03	13.34	9.07	7.08	7.81	13.13	17.57	19.11	17.71	11.27	12.00	14.96
[4,5)	13.89	15.22	12.34	10.26	12.64	16.02	19.95	17.38	16.83	12.24	13.20	15.12
[5,6)	12.41	14.58	16.92	13.18	15.46	15.89	16.38	13.08	14.13	13.26	13.44	12.62
[6,7)	10.56	12.98	16.61	15.06	17.14	14.93	11.38	8.50	9.52	12.86	12.12	9.65
[7,8)	8.84	10.29	15.53	16.52	16.51	13.02	7.52	4.37	6.61	11.79	10.73	7.96
[8,9)	5.97	6.68	9.39	11.79	10.62	7.11	3.16	1.98	3.65	7.88	7.23	5.10
[9,10)	4.32	4.13	6.02	8.87	6.38	3.74	1.57	1.25	2.49	5.75	4.98	3.66
[10,11)	3.13	2.50	2.70	5.17	3.27	2.18	0.73	0.94	1.80	4.09	3.34	2.73
[11,12)	2.30	1.57	1.09	2.41	1.28	1.24	0.51	0.62	1.03	2.88	2.28	1.94
[12,13)	1.84	1.18	0.50	0.94	0.56	0.60	0.37	0.41	0.56	2.19	1.79	1.47
[13,14)	1.17	0.75	0.19	0.24	0.16	0.16	0.21	0.24	0.24	1.33	1.19	0.95
[14,15)	0.77	0.58	0.08	0.11	0.07	0.04	0.16	0.14	0.11	0.92	0.90	0.72
[15,16)	0.48	0.46	0.03	0.06	0.03	0.01	0.13	0.08	0.05	0.63	0.69	0.55
[16,17)	0.29	0.32	0.01	0.03	0.01	0.01	0.10	0.05	0.02	0.43	0.54	0.39
[17, ∞)	0.31	0.37	0.00	0.02	0.00	0.04	0.17	0.05	0.02	0.59	1.37	0.51

Remark: The yellow highlight represents the high-frequency WSRs.

Table 4. Annual and seasonal parameters of observed wind speeds.

Season	Annual	Spring	Summer	Autumn	Winter
MWS (m/s)	5.2503	5.9326	4.4912	5.3854	5.2428
SD (m/s)	2.8103	2.3761	2.3941	3.1001	3.0694
EWS (m/s)	36.8	26.1	36.8	32	25.2
MTI (%)	6.69	5.01	6.69	7.20	7.32

Table 5. Monthly parameters of observed wind speeds.

Month	MWS (m/s)	SD (m/s)	EWS (m/s)	MTI (%)
Jan	5.3038	3.1389	22.1	7.40
Feb	5.3633	2.8825	25.0	6.72
Mar	5.6911	2.2996	18.8	5.05
Apr	6.2222	2.5077	26.1	5.04
May	5.8739	2.2892	17.6	4.87
Jun	5.2333	2.3676	36.8	5.66
Jul	4.3855	2.3024	36.3	6.56
Aug	3.8087	2.3116	24.0	7.59
Sep	4.3213	2.4466	32.0	7.08
Oct	6.0446	3.1622	25.4	6.54
Nov	5.8785	3.3763	25.8	7.18
Dec	5.0746	3.1522	25.2	7.76

Turbulence intensity in this analysis is calculated as the standard deviation of the wind speed (SD_{10min}) in each 10 min period divided by the mean wind speed (MWS_{10min}) in each 10 min period [34]:

$$TI = \frac{SD_{10min}}{MWS_{10min}} \quad (15)$$

The analyses in Tables 4 and 5 show that mean turbulence intensity (MTI) is less than 7.5% due to the low offshore surface roughness and thus weakens the impact of wind wake [35]. The MTIs in each season, as function of wind speed, are shown in Figure 4. The variations by period are not significant compared to the variability of TI at each wind speed. The TIs at low WRSs are highest, decrease rapidly to a minimum of around 4–8 m/s, which is the high-frequency WSRs, and then remain constant.

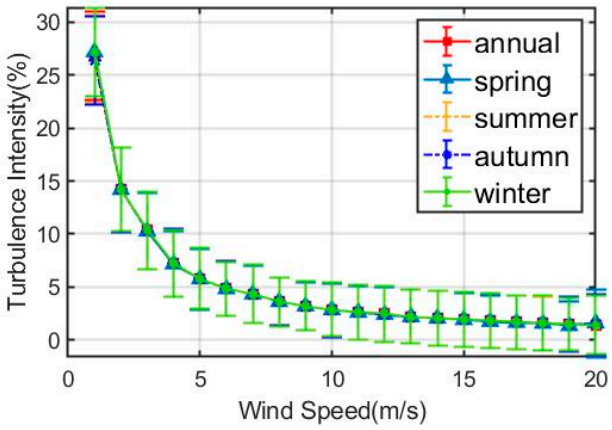

Figure 4. The relationship between turbulence intensity (TI) and wind speed. The solid lines show data binned in 1 m/s classes, where the line shows the mean value and the bars denote plus/minus half a standard deviation (±SD) around the mean.

Figure 5 shows the mean wind speed during each hour of the day (24 h) in each season and month. As shown in Figure 5, the MWS magnitudes in spring are relatively higher and more stable, while those in summer are relatively lower than other seasons. This is similar to the conclusion of Ali et al. [4], who studied a similar location (latitude and longitude of 37.22° N, 126.14° E compared with 38.7° N, 118.7° E in this study). Although the wind speed varies significantly between each hour, it exhibits two distinct patterns. First, the wind speed usually decreases at approximately 04:00 (4 h in Figure 5), reaches the minimum value of the day at approximately 14:00 (14 h in the figure), and then begins to increase. Second, the wind speed at night (20–24 h and 1–8 h) is usually higher than that in the day (8–20 h).

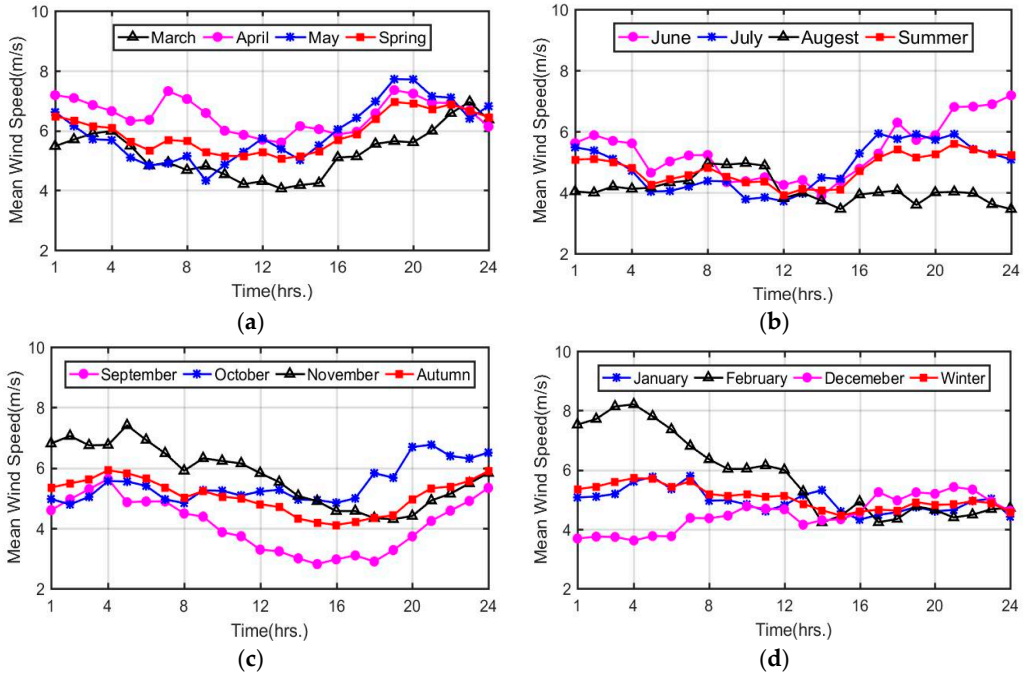

Figure 5. Wind speed variation during each day: (**a**) spring and its three months; (**b**) summer and its three month; (**c**) autumn and its three month; (**d**) winter and its three months.

Figure 6 shows the variations in the average wind angles with each hour of the day (24 h) in different months and seasons. The daily average wind angle fluctuates vertically at approximately 0° (east) between 60° (northeast) and −60° (southeast). As shown in Figures 5 and 6, throughout the year, the wind mainly originates from the east (0°) with a speed ranging from 4 to 8 m/s, which is consistent with the above conclusion.

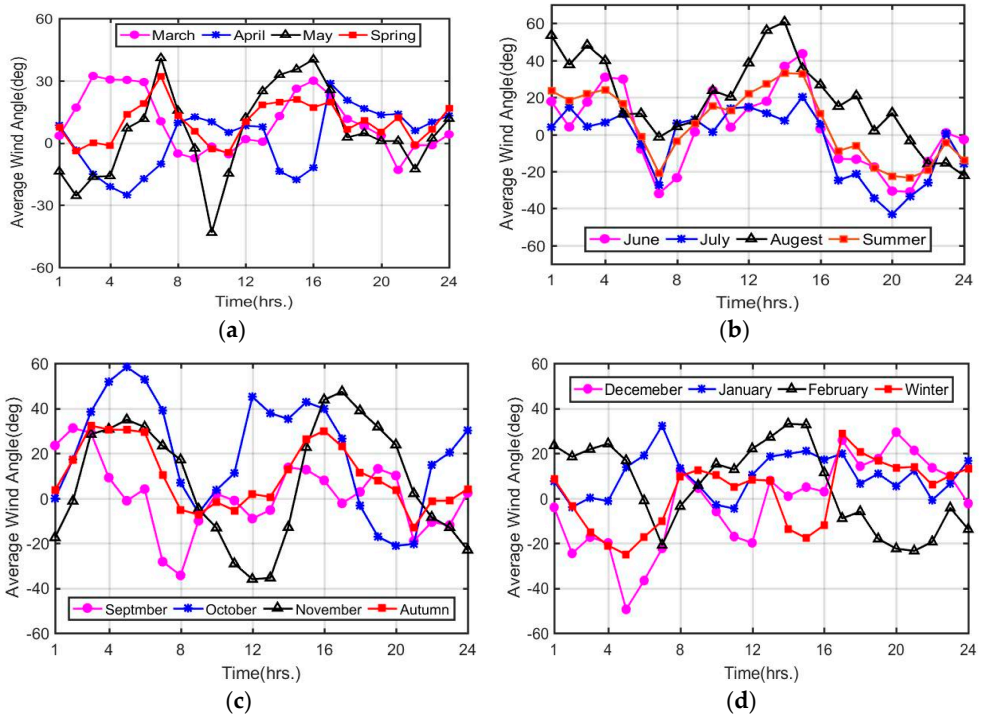

Figure 6. Wind angle variation during each day: (**a**) spring and its three months; (**b**) summer and its three month; (**c**) autumn and its three month; (**d**) winter and its three months.

4.2. Wind Speed Probability Distributions

Wind is highly spatiotemporally variable; thus, it is necessary to understand the wind speed distribution in advance.

Figure 7a shows the Weibull (Wei), Nakagami (Nak), Rician (Ric), and Rayleigh (Ray) probability and cumulative distributions of the observed annual wind speeds. The real data and fitting curves are both presented on the same diagram to allow the differences to be easily distinguished. Figure 7b shows the Q–Q probability plots between the observed annual data and data from the corresponding probability distribution functions. The Q–Q plots could describe a linear relationship between the real data and forecasted values. Figure 8 shows four distributions for the observed seasonal wind speeds, while Tables 6 and 7 present the important parameters of the observed wind speed and four distribution models based on the nonlinear least-squares method. Tables 8 and 9 present the RMSE and R^2 between the observed and predicted values by the four distributions.

Table 6. Parameters of corresponding distributions based on annual and seasonal wind data.

Season		Annual	Spring	Summer	Autumn	Winter
Weibull	k	2.086	2.839	2.174	1.951	1.895
	c	5.851	6.772	5.045	5.818	5.646
Nakagami	μ	1.068	1.753	1.148	0.9751	0.9331
	ω	33.96	43.97	25.04	33.91	32.12
Rician	a	3.375	2.544	2.664	4.099	3.962
	b	3.225	5.334	3.155	0.3342	0.424
Rayleigh	σ	5.864	6.821	5.072	5.805	5.617

Table 7. Parameters of corresponding distributions based on monthly observed wind data.

Month	Weibull		Nakagami		Rician		Rayleigh
	k	***c***	μ	ω	***a***	***b***	σ
Jan	1.81	5.74	0.871	36.8	4.02	0.18	5.68
Feb	2.14	5.83	1.12	33.5	3.15	3.54	5.86
Mar	2.80	6.48	1.7	40.3	2.47	5.07	6.53
Apr	2.84	7.18	1.75	49.4	2.7	5.66	7.21
May	2.94	6.67	1.87	42.6	2.42	5.33	6.73
Jun	2.48	5.93	1.41	33.9	2.56	4.35	5.98
Jul	2.34	4.88	1.29	23.2	2.26	3.42	4.93
Aug	2.03	4.28	1.04	18.2	2.98	0.755	4.29
Sep	1.98	4.75	1	22.5	3.35	0.176	4.74
Oct	2.105	6.589	1.09	43	4.66	0.586	6.61
Nov	2.02	6.23	1.02	38.7	4.33	1.17	6.24
Dec	1.81	5.36	0.873	29.2	3.72	0.642	5.29

Month		Jan	Feb	Mar	Apr	May	Jun	Jul	Aug	Sep	Oct	Nov	Dec
Wei	k	1.81	2.14	2.80	2.84	2.94	2.48	2.34	2.03	1.98	2.105	2.02	1.81
	c	5.74	5.83	6.48	7.18	6.67	5.93	4.88	4.28	4.75	6.589	6.23	5.36
Nak	μ	0.871	1.12	1.70	1.75	1.87	1.41	1.29	1.04	1.00	1.09	1.02	0.873
	ω	36.8	33.5	40.3	49.4	42.6	33.9	23.2	18.2	22.5	43.0	38.7	29.2
Ric	a	4.02	3.15	2.47	2.70	2.42	2.56	2.26	2.98	3.35	4.66	4.33	3.72
	b	0.18	3.54	5.07	5.66	5.33	4.35	3.42	0.755	0.176	0.586	1.17	0.642
Ray	σ	5.68	5.86	6.53	7.21	6.73	5.98	4.93	4.29	4.74	6.61	6.24	5.29

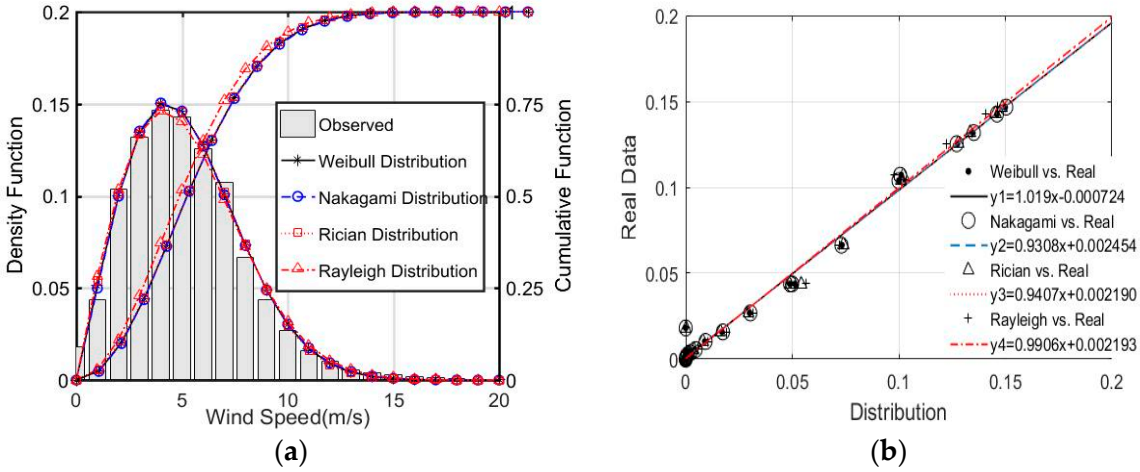

Figure 7. Comparison of the annual wind data and the different distributions: (**a**) annual wind data and the four probability density functions (PDFs) and cumulative distribution functions (CDFs); (**b**) Q–Q plot of the real data and the four distributions used in this study.

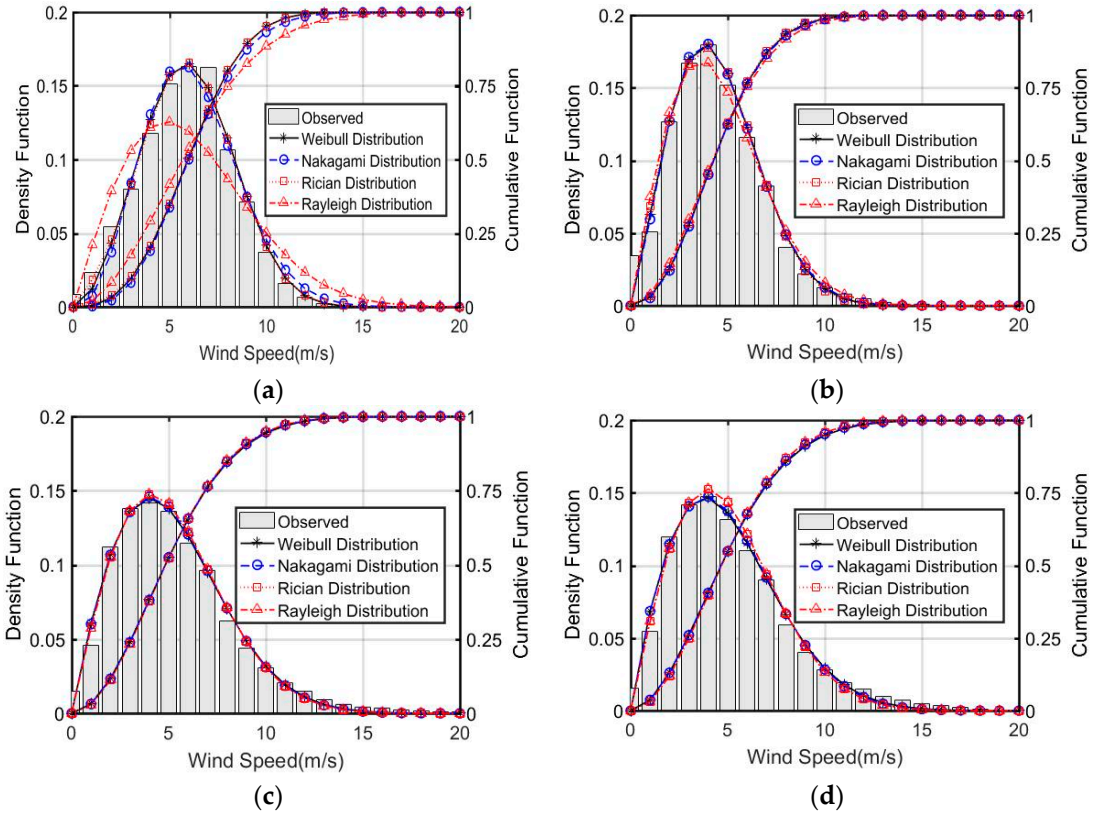

Figure 8. Seasonal wind data and wind speed distributions with different PDFs and CDFs: (**a**) spring; (**b**) summer; (**c**) autumn; (**d**) winter.

Weibull, Nakagami, and Rician distributions all performed well in comparison to the observed wind speed, as indicated by the high $R^2 \geq 97\%$ and low RMSE < 0.008, excluding those in August, which were 0.95 and 0.012, respectively. According to Figure 9, the four distributions did not fit the observed wind speeds in August as accurately due to the high percentage of null winds, which will be improved in future work. In most cases, the R^2 and RMSE of Nakagami distribution were higher and lower, respectively, than those of other distributions. Rayleigh distribution exhibited the poorest R^2 and RMSE. However, this distribution has only one parameter, which allows it to be calculated more quickly. Therefore, Nakagami distribution may be better for assessing wind resources in this region.

Table 8. Error evaluation of PDFs in the whole year and each season.

Distribution	Indicators	Annual	Spring	Summer	Autumn	Winter	Sum
Weibull	RMSE (10^{-3})	4.44	5.155	7.283	4.817	4.843	22.098
	R^2	0.9921	0.9907	0.9829	0.9901	0.9901	3.9538
Nakagami	RMSE (10^{-3})	4.409	5.153	7.123	4.914	5.102	22.292
	R^2	0.9922	0.992	0.9836	0.9897	0.989	3.9543
Rician	RMSE (10^{-3})	4.58	4.19	7.707	4.988	5.625	22.51
	R^2	0.9916	0.9938	0.9809	0.9894	0.9866	3.9507
Rayleigh	RMSE (10^{-3})	4.845	17.4	8.532	4.909	5.539	36.38
	R^2	0.9906	0.8935	0.9765	0.9897	0.9871	3.8468

Table 9. Error evaluation of PDFs in each month.

	Weibull		Nakagami		Rician		Rayleigh	
Month	R^2	**RMSE**	R^2	**RMSE**	R^2	**RMSE**	R^2	**RMSE**
Jan	0.987	0.0054	0.9845	0.0059	0.9747	0.0076	0.9755	0.0074
Feb	0.994	0.0038	0.9946	0.0037	0.9927	0.0043	0.9895	0.0052
Mar	0.989	0.0057	0.9908	0.0056	0.9924	0.0048	0.9007	0.0172
Apr	0.987	0.0060	0.9858	0.0060	0.9903	0.0050	0.8879	0.0172
May	0.992	0.0049	0.9932	0.0051	0.9944	0.0041	0.8784	0.0191
Jun	0.990	0.0054	0.9888	0.0057	0.9896	0.0055	0.9476	0.0124
Jul	0.987	0.0068	0.9874	0.0066	0.985	0.0072	0.9642	0.0111
Aug	0.953	0.0128	0.9539	0.0117	0.9532	0.0128	0.9547	0.0126
Sep	0.984	0.0070	0.9839	0.0071	0.9839	0.0071	0.9845	0.0069
Oct	0.992	0.0041	0.9925	0.0040	0.989	0.0048	0.9894	0.0048
Nov	0.990	0.0046	0.9902	0.0046	0.99	0.0047	0.9903	0.0046
Dec	0.984	0.0062	0.9813	0.0067	0.9723	0.0082	0.9732	0.0081
Sum	11.830	0.0727	11.827	0.0737	11.808	0.0761	11.436	0.1266

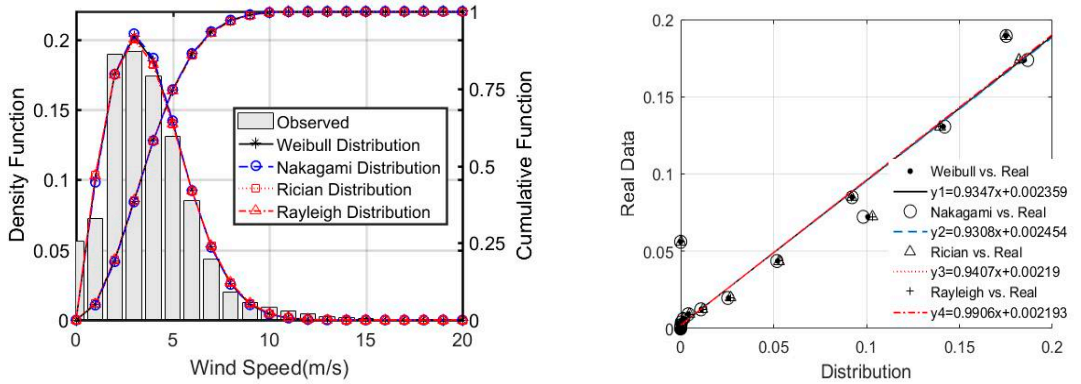

(**a**) (**b**)

Figure 9. Comparisons of the wind data collected in August and those predicted by the different distributions. (**a**) Wind distribution in August against the four PDFs and CDFs; (**b**) Q–Q plot between the real data and four PDFs.

4.3. Wind Potential Analysis at Bohai Bay

The most probable wind speed (v_{mp}), which has the highest percentage of occurrence during a specified time period, and the wind speed carrying the maximum energy (v_{me}), which is usually used as the designed wind speed of wind turbines [36], were introduced to assess the wind resources in Bohai Bay and were determined by the Weibull and Rayleigh distributions [4]:

$$v_{mp-wei} = \mathrm{c}(1 - \frac{1}{k})^{1/k} \quad (16)$$

$$v_{me-wei} = \mathrm{c}(1 + \frac{2}{k})^{1/k} \tag{17}$$

$$v_{mp-ray} = \sigma / \sqrt{2} \tag{18}$$

$$v_{me-ray} = \sqrt{2}\sigma \tag{19}$$

The v_{mp} and v_{me} values determined by the Nakagami and Rician distributions were first used in wind resource assessment and calculated as follows:

$$v_{mp-nak} = (\omega - \frac{\omega}{2\mu})^{1/2} \tag{20}$$

$$v_{me-nak} = (\omega + \frac{\omega}{\mu})^{1/2} \tag{21}$$

Owing to the difficulty of solving and expressing the accurate function, the v_{mp} and v_{me}, determined by Rician distributions, were calculated as follows:

$$I_0\left(\frac{bv_{mp-ric}}{a^2}\right) - \left(\frac{v_{mp-ric}}{a}\right)^2 I_0\left(\frac{bv_{mp-ric}}{a^2}\right) + \frac{bv_{mp-ric}}{a^2} I_1\left(\frac{bv_{mp-ric}}{a^2}\right) = 0 \tag{22}$$

$$4I_0\left(\frac{bv_{me-ric}}{a^2}\right) - \left(\frac{v_{me-ric}}{a}\right)^2 I_0\left(\frac{bv_{me-ric}}{a^2}\right) + \frac{bv_{me-ric}}{a^2} I_1\left(\frac{bv_{me-ric}}{a^2}\right) = 0 \tag{23}$$

The wind power density (WPD) and wind energy density (WED), which are indicators of the power and energy of winds at a particular geographical location, respectively, could also be calculated by the parameters of the distributions and determined by the Weibull and Rayleigh distributions as follows [37]:

$$\mathrm{WPD}_{wei} = \frac{P}{A} = \int_0^\infty \frac{1}{2}\rho v^3 f(v) dv = \frac{1}{2}\rho c^3 \Gamma(1 + \frac{3}{k}) \tag{24}$$

$$\mathrm{WPD}_{Ray} = \frac{3\sqrt{\pi}}{8}\rho\sigma^3 \tag{25}$$

$$\mathrm{WED} = \mathrm{WPD} \cdot T \tag{26}$$

where WPD is the wind power density ($\mathrm{W/m^2}$), WED is the wind energy density ($\mathrm{kWh/m^2}$), T is the time period, and ρ is the air density (assumed to be 1.25 $\mathrm{km/m^3}$) [38]. Similarly, WPD_{Nak} and WED_{Nak} were determined by Nakagami and Rician distributions and used to assess the wind potential, which were calculated as follows:

$$\mathrm{WPD}_{Nak} = \frac{1}{2}\rho\left(\frac{\omega}{\mu}\right)^{\frac{3}{2}} \frac{\Gamma(\mu + \frac{3}{2})}{\Gamma(\mu)} \tag{27}$$

$$\mathrm{WPD}_{Ric} = \frac{\sqrt{2\pi}}{8a}\rho e^{-\frac{b^2}{4a^2}}\left[I_0\left(\frac{b^2}{4a^2}\right)\left(6a^4 + 6I_0 a^2 b^2 + b^4\right) + I_1\left(\frac{b^2}{4a^2}\right)\left(4a^2 b^2 + b^4\right)\right] \tag{28}$$

The observed WPD can be calculated as follows:

$$\mathrm{WPD} = \frac{\sum_{i=1}^{n} 0.5\rho {v_i}^3}{n} \tag{29}$$

where n is the total number of data points, and v_i is the ith entry of the observed wind speed data.

Table 10 summarizes the PDFs, CDFs, and important parameters of wind energy assessment based on the four distributions used in the paper. Tables 11 and 12 show the results of the annual, seasonal, and monthly wind potential assessments based on four distributions. The results of all four estimation methods were similar. The largest v_{mp} and v_{me} values were observed in April, during spring, while the smallest values were observed in August, during autumn. The values of v_{mp} based on Rician

distribution were largest, followed by those based on Weibull and Nakagami distributions, and those based on Rayleigh distribution were lowest, with maximum values of 6.20, 6.27, 5.94, and 5.10 m/s, respectively. The values of v_{me} based on Rayleigh distribution were generally largest, followed by those based on Nakagami and Weibull distributions. Finally, those based on Rician distribution were lowest, with maximum values of 10.20, 8.81, 8.66, and 8.60 m/s, respectively. The forecasted WEDs (kWh/m^2) were highest in April and lowest in August.

Figure 10 presents the seasonal distributions of observed WPDs, which are mostly below 200 W/m^2 in Bohai Bay but are relatively higher during autumn and winter (higher percentage of WPDs over 600 W/m^2) than those in summer. The corresponding prevailing winds carrying the highest WPD blow from the east, as shown in Figure 3. Therefore, Bohai Bay could be considered as a wind class I region (WPD < 200 W/m^2) [39], with east as the predominant energy-flow direction [40].

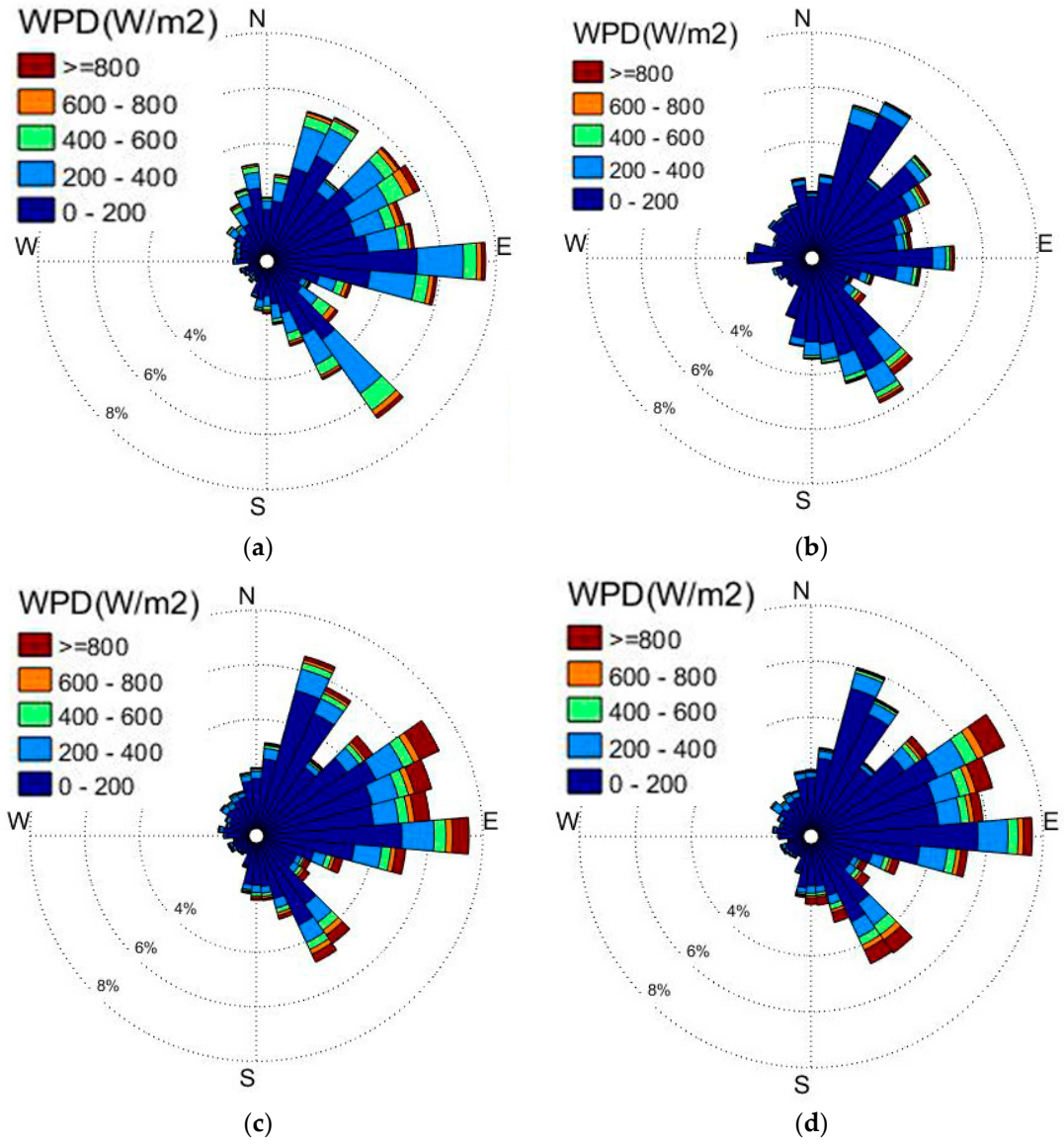

Figure 10. Observed wind power density (WPD) rose diagrams: (**a**) spring; (**b**) summer; (**c**) autumn; (**d**) winter.

Table 10. PDFs, CDFs, and the parameters of wind potential assessment.

Name	PDF	CDF	v_{mp}	v_{me}	WPD
Weibull	$\left(\frac{k}{c}\right)\left(\frac{v}{c}\right)^{k-1}e^{-\left(\frac{v}{c}\right)^{k}}$	$1-e^{-\left(\frac{v}{c}\right)^{k}}$	$c(1-\frac{1}{k})^{1/k}$	$c(1+\frac{2}{k})^{1/k}$	$\frac{1}{2}\rho c^3\Gamma(1+\frac{3}{k})$
Nakagami	$2(\frac{\mu}{\omega})^{\mu}\frac{1}{\Gamma(\mu)}v^{(2\mu-1)}e^{-\frac{\mu v^2}{\omega}}$	$\frac{\gamma(\mu,\frac{\mu}{\omega}v^2)}{\Gamma(\mu)}$	$(\omega-\frac{\omega}{2\mu})^{1/2}$	$(\omega+\frac{\omega}{\mu})^{1/2}$	$\frac{1}{2}\rho\left(\frac{\omega}{\mu}\right)^{\frac{3}{2}}\frac{\Gamma(\mu+\frac{3}{2})}{\Gamma(\mu)}$
Rician	$\frac{x}{a^2}\exp\left(\frac{-(x^2+b^2)}{2a^2}\right)I_0\left(\frac{bx}{a^2}\right)$	$1-Q_1\left(\frac{b}{a},\frac{x}{a}\right)$	$I_0\left(\frac{bv_{mp-ric}}{a^2}\right)\left[1-\left(\frac{v_{mp-ric}}{a}\right)^2\right]+\frac{bv_{mp-ric}}{a^2}I_1\left(\frac{bv_{mp-ric}}{a^2}\right)=0$	$I_0\left(\frac{bv_{me-ric}}{a^2}\right)\left[4-\left(\frac{v_{me-ric}}{a}\right)^2\right]+\frac{bv_{me-ric}}{a^2}I_1\left(\frac{bv_{me-ric}}{a^2}\right)=0$	$\frac{\sqrt{2\pi}}{8a}\rho e^{-\frac{b^2}{4a^2}}\left[I_0\left(\frac{b^2}{4a^2}\right)\left(6a^4+6I_0a^2b^2+b^4\right)+I_1\left(\frac{b^2}{4a^2}\right)\left(4a^2b^2+b^4\right)\right]$
Rayleigh	$\frac{x}{\sigma^2}e^{-\frac{x^2}{2\sigma^2}}$	$1-e^{-\frac{x^2}{2\sigma^2}}$	$\sigma/\sqrt{2}$	$\sqrt{2}\sigma$	$\frac{3\sqrt{\pi}}{8}\rho\sigma^3$

Table 11. Annual and seasonal wind potential assessment.

Time	Weibull			Nakagami			Rician			Rayleigh		
	v_{mp}	v_{me}	WED	v_{mp}	v_{me}	WED	v_{mp}	v_{me}	WED	v_{mp}	v_{me}	WED
Annual	4.3	8.1	115.0	4.3	8.1	116.7	4.3	8.1	112.1	4.2	8.3	120.6
Spring	5.8	8.2	143.3	5.6	8.3	143.2	5.9	8.1	142.4	4.8	9.7	189.8
Summer	3.8	6.8	70.9	3.8	6.8	72.8	3.9	6.8	68.5	3.6	7.2	78.1
Autumn	4.0	8.4	121.0	4.1	8.3	118.8	4.1	8.2	117.1	4.1	8.2	117.0
Winter	3.8	8.3	114.3	3.9	8.2	110.6	4.0	8.0	106.1	4.0	7.9	106.0

Remark: v_{mp} (m/s), v_{me} (m/s), WED (kWh/m^2).

Table 12. Monthly wind potential assessment.

Time	Weibull			Nakagami			Rician			Rayleigh		
	v_{mp}	v_{macE}	WED	v_{mp}	v_{macE}	WED	v_{mp}	v_{macE}	WED	v_{mp}	v_{macE}	WED
Jan	3.7	8.7	127.0	4.0	8.9	137.8	4.0	8.0	109.8	4.0	8.0	109.7
Feb	4.3	7.9	110.7	4.3	8.0	113.4	4.4	7.9	106.9	4.1	8.3	120.1
Mar	5.5	7.9	126.4	5.3	8.0	126.1	5.6	7.8	125.2	4.6	9.2	166.6
Apr	6.2	8.7	170.7	5.9	8.8	171.3	6.2	8.6	169.8	5.1	10.2	224.4
May	5.8	8.0	134.9	5.6	8.1	135.1	5.8	7.9	134.9	4.8	9.5	182.5
Jun	4.8	7.5	103.7	4.7	7.6	110.7	4.9	7.4	100.3	4.2	8.5	128.1
Jul	3.8	6.4	60.2	3.8	6.4	63.4	3.9	6.2	56.2	3.5	7.0	71.7
Aug	3.1	6.0	46.2	3.1	6.0	46.0	3.0	6.1	47.1	3.0	6.1	47.1
Sept	3.3	6.8	64.9	3.4	6.7	63.6	3.4	6.7	64.0	3.4	6.7	63.8
Oct	4.9	9.1	162.6	4.8	9.1	165.5	4.7	9.4	173.1	4.7	9.4	173.1
Nov	4.4	8.8	143.7	4.5	8.8	143.4	4.4	8.8	145.2	4.4	8.8	145.2
Dec	3.4	8.1	103.6	3.5	7.9	97.2	3.7	7.5	88.8	3.7	7.5	88.7

4.4. Evaluation of the Probability Density Functions

Table 13 compares observed and forecasted WPDs during different time spans, such as the whole year, four seasons, and 12 months. The error percentage is calculated as follows:

$$\text{ERROR} = \left(\frac{\textit{observed}\ \text{WPD} - \textit{forecasted}\ \text{WPD}}{\textit{observed}\ \text{WPD}}\right)100\% \tag{30}$$

Table 13 indicates that the given PDFs can all accurately assess the wind potential and forecast the wind characteristics in Bohai Bay. However, the forecasted WPDs were slightly smaller than the observed WPDs in most cases as the forecasted WPD calculation does not consider extreme wind speeds, such as those during typhoons. Nakagami distribution performed best for forecasting WPD, followed by Weibull, Rician, and Rayleigh distribution, according to the error sum values. The performances of the different distributions in WPD were similar to those for the wind speed distributions.

Table 13. Evaluation of the errors between the observed and forecasted WPD.

Time	Real	Wei	Error%	Nak	Error%	Ric	Error%	Ray	Error%
Annual	180.5	159.7	11.5	162.1	10.2	155.7	13.8	167.5	7.2
Spring	194.1	199.0	−2.5	198.9	−2.5	197.8	−1.9	263.7	−35.9
Summer	111.3	98.4	11.6	101.1	9.1	95.1	14.5	108.4	2.6
Autumn	215.4	168.1	22.0	165.0	23.4	162.7	24.5	162.5	24.5
Winter	201.8	158.8	21.3	153.6	23.9	147.4	26.9	147.2	27.0
Jan	209.8	176.4	15.9	191.4	8.8	152.6	27.3	152.3	27.4
Feb	195.4	153.8	21.3	157.5	19.4	148.5	24.0	166.9	14.6
Mar	172.9	175.6	−1.6	175.1	−1.3	173.9	−0.6	231.5	−33.9
Apr	224.0	237.1	−5.9	237.9	−6.2	235.8	−5.3	311.7	−39.2
May	184.9	187.4	−1.3	187.6	−1.5	187.4	−1.3	253.5	−37.1
Jun	148.2	144.0	2.8	153.7	−3.8	139.3	6.0	177.9	−20.1
Jul	105.2	83.7	20.5	88.0	16.4	78.1	25.8	99.6	5.4
Aug	81.5	64.2	21.2	64.0	21.5	65.5	19.7	65.4	19.7
Sept	107.3	90.1	16.1	88.4	17.6	88.9	17.2	88.5	17.5
Oct	268.4	225.8	15.9	229.8	14.4	240.5	10.4	240.4	10.4
Nov	282.4	199.6	29.3	199.2	29.5	201.7	28.6	201.7	28.6
Dec	199.4	143.8	27.9	134.9	32.3	123.4	38.1	123.2	38.2
Sum			248.4		241.6		285.9		389.2

5. Conclusions

In this study, the wind characterization and energy potential of Bohai Bay, China, during 2015–2016 at different timescales, such as seasons, months, and hours, were analyzed in detail to more accurately predict the wind behavior. Based on the analysis and results, the following conclusions can be drawn:

1. In Bohai Bay, the wind mainly blows from the east (E −15°–45°), followed by the southeast (SE −55°−−45°) and northeast (NE 55°–75°). The winds speed in Bohai Bay is mostly lower than 12 m/s, generally in the range of 4–8 m/s, and the main wind speed ranges in April and October are higher than those in August and December. However, in summer, the magnitude of average wind speeds is lower but the magnitude of extreme wind speeds is higher due to the occurrence of monsoons, such as typhoons. The wind speed from 20:00 to 08:00 is higher than that from 08:00 to 20:00 and exhibits a sinusoidal pattern over each hour of each day. The turbulence intensity is low due to the low surface roughness and mainly depends on wind speeds instead of periods.
2. Weibull, Nakagami, Rician, and Rayleigh distributions all performed well in comparison to the observed wind speed, where Nakagami and Rician distributions were first introduced in the field of wind energy and performed well in predicting the wind speed distributions. However, none of the distributions fit the wind speed distributions in August due to the high percentage of null winds.

3. The most probable wind speed, the most energy-carrying wind speed, and the wind power density based on Nakagami (Rician) distributions were first proposed and used to assess the wind potential and forecast the wind characteristics in Bohai Bay. Nakagami distribution performed better than the other three distributions in forecasting WPD. Based on the results of the analysis, Bohai Bay can be considered as a wind class I region, with east as the dominant direction as the corresponding WPD is mostly below 200 W/m^2 and mainly faces the east.

Author Contributions: All authors contributed to the research in this paper. J.Y. designed the study. Y.F. searched the literature, analyzed the data and wrote the paper; Y.Y. designed the study and analyzed the data; S.W., Y.W., S.G. and M.Y. extracted the data and analyzed the data. M.L. provided the data.

Funding: This research was funded by the National Key R&D Program of China (2018YFC0310502), the National Science and Technology Major Project (Grant No. 2016ZX05028005-004), the National Natural Science Foundation of China (Grant No. 51879189), and the National Natural Science Foundation of China for Youth (Grant No. 51609169).

Acknowledgments: These supports were gratefully acknowledged. We also express special thanks to the reviewers and editors for their constructive comments and suggestions on this manuscript and to Yue Xiaoxue and Zhou Huan for their help in revising the paper.

Conflicts of Interest: The authors declare no conflict of interest.

Notations and Abbreviations

PDF	Probability density function
R^2	Correlation coefficient
FPSO	Floating production storage and offloading
k	Weibull shape parameter
μ	Nakagami shape parameter
Γ	Gamma function
a	Rician scale parameter
I_α	The modified Bessel function of the first-kind with an order of α
σ	Rayleigh scale parameter (m/s)
Nak	Nakagami
Ric	Rician
WSR	Wind speed range
SD	Standard deviation
v_{me}	Most energy-carrying wind speed
WED	Wind energy density (kWh/m^2)
TI	Turbulence intensity
CDF	Cumulative distribution function
RMSE	Root mean square error
ρ	Air density (kg/m^3)
c	Weibull scale parameter (m/s)
ω	Nakagami scale parameter
γ	Upper incomplete gamma function
b	Rician location parameter
Q_1	Marcum Q-function
v	Wind speed (m/s)
Wei	Weibull
Ray	Rayleigh
MWS	Mean wind speed
v_{mp}	The most probable wind speed
WPD	Wind speed density (W/m^2)
T	Time period
MTI	Mean turbulence intensity

References

1. Global Wind Energy Council. *Global Wind Energy Report: Annual Market Update 2017*; Global Wind Energy Council: Bruxelles, Belgium, 2018.
2. Zhao, X.; Ren, L. Focus on the development of offshore wind power in China: Has the golden period come? *Renew. Energy* **2015**, *81*, 644–657. [CrossRef]
3. Niu, T.; Wang, J.; Lu, H.; Du, P. Uncertainty modeling for chaotic time series based on optimal multi-input multi-output architecture: Application to offshore wind speed. *Energy Convers. Manag.* **2018**, *156*, 597–617. [CrossRef]
4. Ali, S.; Lee, S.M.; Jang, C.M. Statistical analysis of wind characteristics using Weibull and Rayleigh distributions in Deokjeok-do Island–Incheon, South Korea. *Renew. Energy* **2018**, *123*, 652–663. [CrossRef]
5. Lun, I.Y.F.; Lam, J.C. A study of Weibull parameters using long-term wind observations. *Renew. Energy* **2000**, *20*, 145–153. [CrossRef]
6. Baseer, M.A.; Meyer, J.P.; Rehman, S.; Alam, M.M. Wind power characteristics of seven data collection sites in Jubail, Saudi Arabia using Weibull parameters. *Renew. Energy* **2017**, *102*, 35–49. [CrossRef]
7. Rodriguez-Hernandez, O.; Jaramillo, O.A.; Andaverde, J.A.; del Río, J.A. Analysis about sampling, uncertainties and selection of a reliable probabilistic model of wind speed data used on resource assessment. *Renew. Energy* **2013**, *50*, 244–252. [CrossRef]
8. Wais, P. Two and three-parameter Weibull distribution in available wind power analysis. *Renew. Energy* **2017**, *103*, 15–29. [CrossRef]
9. Seguro, J.V.; Lambert, T.W. Modern estimation of the parameters of the Weibull wind speed distribution for wind energy analysis. *J. Wind Eng. Ind. Aerodyn.* **2000**, *85*, 75–84. [CrossRef]
10. Zheng, C.W.; Li, C.Y.; Pan, J.; Liu, M.Y.; Xia, L.L. An overview of global ocean wind energy resource evaluations. *Renew. Sustain. Energy Rev.* **2016**, *53*, 1240–1251. [CrossRef]
11. Shu, Z.R.; Li, Q.S.; Chan, P.W. Statistical analysis of wind characteristics and wind energy potential in Hong Kong. *Energy Convers. Manag.* **2015**, *101*, 644–657. [CrossRef]
12. Gao, X.; Yang, H.; Lu, L. Study on offshore wind power potential and wind farm optimization in Hong Kong. *Appl. Energy* **2014**, *130*, 519–531. [CrossRef]
13. Wang, J.; Qin, S.; Jin, S.; Wu, J. Estimation methods review and analysis of offshore extreme wind speeds and wind energy resources. *Renew. Sustain. Energy Rev.* **2015**, *42*, 26–42. [CrossRef]
14. Zhang, H.; Yu, Y.J.; Liu, Z.Y. Study on the Maximum Entropy Principle applied to the annual wind speed probability distribution: A case study for observations of intertidal zone anemometer towers of Rudong in East China Sea. *Appl. Energy* **2014**, *114*, 931–938. [CrossRef]
15. Chang, R.; Zhu, R.; Badger, M.; Hasager, C.B.; Xing, X.; Jiang, Y. Offshore wind resources assessment from multiple satellite data and WRF modeling over South China Sea. *Remote Sens.* **2015**, *7*, 467–487. [CrossRef]
16. Wan, Y.; Fan, C.; Dai, Y.; Li, L.; Sun, W.; Zhou, P.; Qu, X. Assessment of the joint development potential of wave and wind energy in the South China Sea. *Energies* **2018**, *11*, 398. [CrossRef]
17. Ouarda, T.B.M.J.; Charron, C.; Shin, J.Y.; Marpu, P.R.; Al-Mandoos, A.H.; Al-Tamimi, M.H.; Ghedira, H.; Al Hosaryc, T.N. Probability distributions of wind speed in the UAE. *Energy Convers. Manag.* **2015**, *93*, 414–434. [CrossRef]
18. Akgül, F.G.; Şenoğlu, B.; Arslan, T. An alternative distribution to Weibull for modeling the wind speed data: Inverse Weibull distribution. *Energy Convers. Manag.* **2016**, *114*, 234–240. [CrossRef]
19. Mohammadi, K.; Alavi, O.; Mostafaeipour, A.; Goudarzi, N.; Jalilvan, M. Assessing different parameters estimation methods of Weibull distribution to compute wind power density. *Energy Convers. Manag.* **2016**, *108*, 322–335. [CrossRef]
20. Hennessey, J.P., Jr. Some aspects of wind power statistics. *J. Appl. Meteorol.* **1977**, *16*, 119–128. [CrossRef]
21. Deaves, D.M.; Lines, I.G. On the fitting of low mean windspeed data to the Weibull distribution. *J. Wind Eng. Ind. Aerodyn.* **1997**, *66*, 169–178. [CrossRef]
22. Kumar, M.B.H.; Balasubramaniyan, S.; Padmanaban, S.; Holm-Nielsen, J.B. Wind Energy Potential Assessment by Weibull Parameter Estimation Using Multiverse Optimization Method: A Case Study of Tirumala Region in India. *Energies* **2019**, *12*, 2158. [CrossRef]
23. Carta, J.A.; Ramirez, P.; Velazquez, S. A review of wind speed probability distributions used in wind energy analysis: Case studies in the Canary Islands. *Renew. Sustain. Energy Rev.* **2009**, *13*, 933–955. [CrossRef]

24. Chang, T.P. Estimation of wind energy potential using different probability density functions. *Appl. Energy* **2011**, *88*, 1848–1856. [CrossRef]
25. Jiang, H.; Wang, J.; Wu, J.; Geng, W. Comparison of numerical methods and metaheuristic optimization algorithms for estimating parameters for wind energy potential assessment in low wind regions. *Renew. Sustain. Energy Rev.* **2017**, *69*, 1199–1217. [CrossRef]
26. Nakagami, M. The m-distribution—A general formula of intensity distribution of rapid fading. In Proceedings of the Symposium Held at the University of California, Los Angeles, CA, USA, 18–20 June 1958; pp. 3–36.
27. de Queiroz, W.J.L.; de Almeida, D.B.T.; Madeiro, F.; Lopes, W.T.A. Signal-to-noise ratio estimation for M-QAM signals in $\eta-\mu$ and $\kappa-\mu$ fading channels. *EURASIP J. Adv. Signal Process.* **2019**, *2019*, 20. [CrossRef]
28. Odeyemi, K.O.; Owolawi, P.A. Selection combining hybrid FSO/RF systems over generalized induced-fading channels. *Opt. Commun.* **2019**, *433*, 159–167. [CrossRef]
29. Marie-Helene, R.C.; Francois, D.; Gilles, S.; Guy, C. Assessment of carotid artery plaque components with machine learning classification using homodyned-K parametric maps and elastograms. *IEEE Trans. Ultrason. Ferroelectr. Freq. Control* **2018**. [CrossRef]
30. Rice, S.O. Mathematical Analysis of Random Noise. *Bell Syst. Tech. J.* **1945**, 23–24. [CrossRef]
31. Le Khoa, N. A review of selection combining receivers over correlated Rician fading. *Digit. Signal Process.* **2019**, *83*, 1–22.
32. Leung, D.Y.C.; Yang, Y. Wind energy development and its environmental impact: A review. *Renew. Sustain. Energy Rev.* **2012**, *16*, 1031–1039. [CrossRef]
33. *Turbines—Part, W. 12-1: Power Performance Measurements of Electricity Producing Wind Turbines*; American National Standards Institute: Washington, DC, USA, 2005.
34. Hansen, K.S.; Barthelmie, R.J.; Jensen, L.E.; Sommer, A. The impact of turbulence intensity and atmospheric stability on power deficits due to wind turbine wakes at Horns Rev wind farm. *Wind Energy* **2012**, *15*, 183–196. [CrossRef]
35. Barthelmie, R.J.; Hansen, K.S.; Pryor, S.C. Meteorological Controls on Wind Turbine Wakes. *Proc. IEEE* **2013**, *101*, 1010–1019. [CrossRef]
36. Jamil, M.; Parsa, S.; Majidi, M. Wind power statistics and an evaluation of wind energy density. *Renew. Energy* **1995**, *6*, 623–628. [CrossRef]
37. Celik, A.N. A statistical analysis of wind power density based on the Weibull and Rayleigh models at the southern region of Turkey. *Renew. Energy* **2004**, *29*, 593–604. [CrossRef]
38. Zheng, C.; Pan, J.; Li, J. Assessing the China Sea wind energy and wave energy resources from 1988 to 2009. *Ocean Eng.* **2013**, *65*, 39–48. [CrossRef]
39. Oh, K.Y.; Kim, J.Y.; Lee, J.K.; Ryu, M.S.; Lee, J.S. An assessment of wind energy potential at the demonstration offshore wind farm in Korea. *Energy* **2012**, *46*, 555–563. [CrossRef]
40. Elliott, D.L.; Holladay, C.G.; Barchet, W.R.; Foote, H.P.; Sandusky, W.F. *Wind Energy Resource Atlas of the United States*; Pacific Northwest Lab.: Richland, WA, USA, 1987.